Electronic structure of superconducting multilayers

H. Plehn, O.-J. Wacker, and R. Kümmel
Physikalisches Institut der Universität Würzburg, D-97074 Würzburg, Germany
(Received 8 November 1993)

The Bloch waves, the energy bands, and the local and global densities of states are computed for superconducting multilayers in which the Fermi energy in the superconducting (S) layers, ε_{FS}, may exceed the one in the normal (N) layers, ε_{FN}. Self-consistent pair potentials and their equivalent square-well representations are considered. If the S-layer thickness exceeds several coherence lengths the densities of states exhibit the subgap peak (besides the BCS peak) and the Tomasch-McMillan-Anderson oscillations known from SNS junctions. These features, due to off–diagonal (Andreev) scattering, decrease with increasing ratio $\varepsilon_{FS}/\varepsilon_{FN}$ because of the competition from diagonal scattering. The temperature dependence of the energetic position of the subgap peak is weaker than that of the BCS peak. In multilayers with S-layer thickness of the order of magnitude of one coherence length and $\varepsilon_{FS}/\varepsilon_{FN} \gg 1$, the local density of states is BCS-like in the S layers and normal-metal-like in the N layers. This is due to electron localization in the S layers and consistent with recent scanning tunneling microscope conductance measurements in $YBa_2Cu_3O_7$.

I. INTRODUCTION

Superconducting multilayers and their electronic structure were discussed theoretically by Andreev[1] when considering the intermediate state in type-I superconductors. In further studies Kronig-Penney and more general models for the pair potential have been used.[2–5] Experimentally, superlattices formed by superconductors (S) and normal metals[6–8] (N) or semiconductors[9,10] have been investigated with respect to their thermodynamic and transport properties. After the discovery of the high-temperature superconductors (HTSC) superconducting multilayers have received special attention again: On the one hand in the form of superlattices artificially prepared from different cuprates[11–14] and on the other hand as models that might facilitate the understanding of the intrinsically layered structure of the HTSC.[4,15–19] Such modeling has recently found rather direct experimental support when Tanaka *et al.*[20] discovered that bulk single grain $YBa_2Cu_3O_7$ specimen exhibit alternating metallic and BCS-like scanning tunneling conductance spectra with a periodicity of 0.8 ± 0.2 nm. Furthermore, in Bi-Sr-Ca-Cu-O (BSCCO) films[21] and single crystals[22,23] a significant deviation of the temperature dependence of the measured gaps from the BCS behavior is observed; see also Ref. 24. In addition, in the single-crystal BSCCO tunneling and Raman spectroscopy reveal two gaps related to anisotropy.[22,23] The anisotropy and the temperature dependence of the in-plane energy gap in $YBa_2Cu_3O_{7-\delta}$ have been measured by Polturak *et al.*[25] using Andreev reflections.

Andreev reflections are the fundamental mechanism that determines the electronic structure of the multilayers with equal Fermi energies treated in Refs. 2–5. In this paper we extend the investigation to multilayers where the Fermi energies in the S and N layers, ε_{FS} and ε_{FN}, may be very different. We do not rely exclusively on the Kronig-Penney model but rather investigate multilayers with self-consistent pair potentials, too. These are discussed in Sec. II, and in Sec. III A we show that equivalent periodic square well representations of them are possible and how they can be constructed. In Sec. III B we compute the quasiparticle wave functions, the energy bands, and the global as well as the local densities of states for different N- and S-layer thicknesses, different ratios of $\varepsilon_{FS}/\varepsilon_{FN}$ and temperatures in the range $0 < T < T_C$. The combined analytical and numerical methods also work in the case of Fermi energies so small that quasiclassical approximations break down. In the Discussion our results are compared with recent experiments on HTSC with emphasis on localization effects due to Andreev scattering and the mismatch of wave vectors parallel to the N-S interfaces.[26]

II. MATERIAL PARAMETERS AND PAIR POTENTIALS

We consider a system of alternating superconducting and normal layers, which is translationally invariant in x and y directions, and which has the periodicity length $d = a + b$ in the z direction. In the superconducting layers, each of thickness b, the pairing interaction is isotropic. The conduction-band electrons of the normal and the superconducting layers are described by dispersion relations of free electrons with equal effective masses m. The Fermi energies of the S layers, ε_{FS}, may, in general, be larger than those of the N layers, ε_{FN}. As in Ref. 27, the spatial variation of the lower conduction-band edges is modeled by step functions, whereas the z dependence of the pair potential $\Delta(z)$, calculated self-consistently for $\varepsilon_{FS} = \varepsilon_{FN}$, and its equivalent square-well representation are shown in Fig. 1. For $\varepsilon_{FS} > \varepsilon_{FN}$ our computations of self-consistent pair potentials indicate

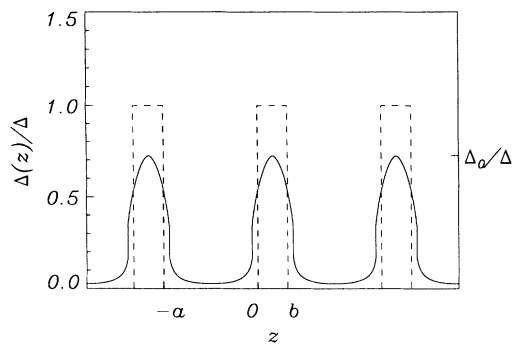

FIG. 1. Self-consistent pair potential (solid line) and its equivalent square-well representation (dashed line) $\Delta(z)$ of a superconducting multilayer with constant Fermi energy; $T_{CN} = 0.1\,T_{CS}$, $a = 6\,\xi_0$, $b = 3\,\xi_0$, $\xi_0 = \hbar^2 k_{FS}/\pi m \Delta(0)$, $\Delta(0) = 1.76\,k_B T_{CS}$, $\Delta = \Delta(0.5\,T_{CS}) = 0.95\,\Delta(0)$

that the square-well representation becomes the better the larger $\varepsilon_{FS}/\varepsilon_{FN}$, see Fig. 2. This is in accordance with Kieselmann's results for proximity contacts.[28]

Similar to Kieselmann's and Ashida's *et al.* calculations for proximity[28] and double-layer[29,30] contacts, our self-consistent computations of multilayer pair potentials are performed with the help of the quasiclassical Green's functions $\hat{g}$. In the weak-coupling limit they obey the equations[28]

$$[i\hbar\omega_n\hat{\tau}_3 - \hat{\Delta}(z), \hat{g}(\hat{\mathbf{k}}, z; \omega_n)] + i(\hat{\mathbf{k}}\cdot\hat{\mathbf{z}})\hbar v_F \frac{d}{dz}\hat{g}(\hat{\mathbf{k}}, z; \omega_n) = 0. \quad (1)$$

Here $\omega_n = (2n-1)\pi k_B T/\hbar$ are the Matsubara frequencies, $v_F(z)$ is the Fermi velocity, $\hat{\tau}_i$ are the Pauli matrices, $\hat{\mathbf{k}}$ is the unit vector in momentum direction, $\hat{\mathbf{z}}$ is the unit vector in z direction, and $[A, B] = AB - BA$. The matrix $\hat{\Delta}$ of the pair potential is given by

$$\hat{\Delta}(z) = \begin{pmatrix} 0 & \Delta(z) \\ -\Delta^*(z) & 0 \end{pmatrix} \quad (2)$$

and is subject to the self-consistency condition

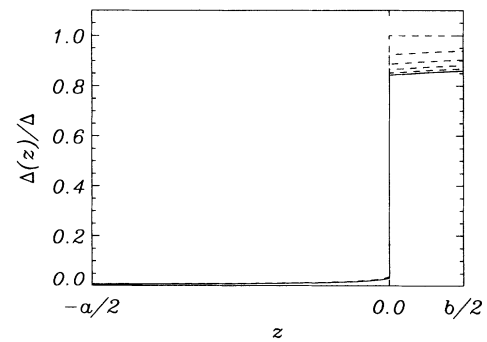

FIG. 2. Self-consistent pair potential for a superconducting double layer with infinite walls at $z = -a/2 = 2\,\xi_0$ and $z = b/2 = 0.5\,\xi_0$. The dashed lines (visible in the range $0 < z < b/2$) show the iterative approach to the self-consistent form; $T_{CN} = T = 0$, $\varepsilon_{FS}/\varepsilon_{FN} = 2$.

$$\Delta(z) = \frac{k_B T \sum_n \int d\Omega_k (4\pi)^{-1} \mathrm{Tr}[\hat{g}(\hat{\mathbf{k}}, z, \omega_n)(\hat{\tau}_1 - i\hat{\tau}_2)]}{\ln[T/T_C(z)] + \sum_n 1/(n-0.5)} \quad (3)$$

with the z-dependent critical temperature

$$T_C(z) = \begin{cases} T_{CN} & \text{in } N \\ T_{CS} & \text{in } S. \end{cases} \quad (4)$$

The solid angle integration is over all momentum directions $\hat{\mathbf{k}}$. The summation Σ_n over the Matsubara frequencies can be cut off at $\hbar\omega_n = \hbar\omega_c \approx 10\,k_B T_C$.[28,31] [Eq. (3) results from a combination of Kieselmann's[28] Eqs. (2.6c) and (2.7b). It has been extended by Bruder[31] to the case of anisotropic pairing interactions.]

In computing $\hat{g}$ and the pair potentials $\Delta(z)$ shown in Figs. 1 and 2 we proceed similarly to Refs. 28 and 31: Defining as the interfaces between the N and the S layers the points where $T_C(z)$ jumps from $T_{CN} < T_{CS}$ to T_{CS}, we compute iteratively solutions of Eqs. (1) and (3) in one N- and one S-layer of thickness $a/2$ and $b/2$, respectively, using the nonlinear boundary conditions[28,32] for $\hat{g}$ at $z = 0$, starting with a steplike pair potential, which vanishes in the N layer, until self-consistency is reached. However, the fact that the N and the S layers are part of a multilayer system is taken into account by including also the solutions for $\hat{g}$, which increase exponentially in S. These solutions, which are left out in the calculations for half-infinite S layers,[28,31] are linearly combined with the exponentially decaying and constant solutions, and this linear combination is subject to the boundary condition of specular reflection in $z = b/2$. The same boundary condition applies at $z = -a/2$. Specular reflection at the system boundaries, i.e., the vanishing of the linear combinations of the quasiparticle wave-functions from which the Green's functions are built up, is assumed by Ashida *et al.*[29] in their considerations of double-layer systems; according to them the periodic continuation of a pair potential calculated self-consistently with these conditions for an N-S-layer system with $\varepsilon_{FS} = \varepsilon_{FN}$ is the pair potential of a multilayer system like the one shown in Fig. 1. For the case $\varepsilon_{FS} \neq \varepsilon_{FN}$ Ashida *et al.*,[30] calculating the transition temperature for double layers, point out that their theory can also be applied to multilayers with appropriate continuation of the double-layer self-consistent pair potential. Thus, we are confident that our conclusion indicated above that square-well pair potentials are rather good approximations of self-consistent pair potentials like the one shown in Fig. 2 if $\varepsilon_{FS} > \varepsilon_{FN}$, holds for multilayers indeed. The square-well shape of the pair potential in this case is due to the localization of all those quasiparticles in the S layers whose momenta $\hbar\mathbf{k}_\varrho$ parallel to the N-S interface exceed the Fermi momentum in the N layers and which are therefore specularly reflected; thus the pair potential in the S layers becomes similar to the one of a superconducting film. For multilayers with $\varepsilon_{FS} = \varepsilon_{FN}$, where the self-consistent pair potential deviates significantly from the square-well form, see Fig. 1, we will see in the next section that square-well representations with effective layer thicknesses are nevertheless acceptable for the computation of energy bands and densities of states.

III. ENERGY BANDS AND DENSITIES OF STATES

A. Sensitivity with respect to self-consistency

We use the Bogoliubov–de Gennes equations (BdGE) with the pair potentials computed in Sec. II. This is convenient because a Wentzel-Kramers-Brillouin-Jeffreys (WKBJ) method of computing quasiparticle wave functions and energies from BdGE with arbitrary spatial variations of the pair potential has been developed before.[3,33,34] Different Fermi energies in N and S are taken into account directly by a spatially varying scalar potential $U(z)$; there is no need to introduce a reflection coefficient R, which enters the boundary conditions for the quasiclassical Green's functions.[28–31,35] Furthermore, the method of the quasiclassical Green's functions breaks down if the Fermi energy does not exceed the pair potential considerably — a situation that may be relevant in the HTSC — whereas exact solutions of the BdGE can be calculated also in the case of small Fermi energies, if square-well-like periodic pair potentials are valid approximations of $\Delta(z)$.

For the quasiparticle wave functions with the electron and hole components $u(\mathbf{r})$ and $v(\mathbf{r})$ we make the ansatz

$$\begin{pmatrix} u(\mathbf{r}) \\ v(\mathbf{r}) \end{pmatrix} = \begin{pmatrix} u(z) \\ v(z) \end{pmatrix} e^{i\mathbf{k}_\varrho \boldsymbol{\varrho}}, \tag{5}$$

where $\mathbf{k}_\varrho = \mathbf{e}_x k_x + \mathbf{e}_y k_y$ is the wave vector of propagation parallel to the N-S interfaces and $\boldsymbol{\varrho} = \mathbf{e}_x x + \mathbf{e}_y y$. The $u(z)$ and $v(z)$ satisfy the one-dimensional BdGE

$$Eu(z) = \mathcal{H}_e u(z) + \Delta(z) v(z), \tag{6a}$$

$$Ev(z) = -\mathcal{H}_e v(z) + \Delta(z) u(z), \tag{6b}$$

where

$$\mathcal{H}_e \equiv -\frac{\hbar^2}{2m}\frac{\partial^2}{\partial^2 z} + \frac{\hbar^2 k_\varrho^2}{2m} + U(z) - \mu. \tag{7}$$

In the N layers we have $\mu - U(z) \equiv \varepsilon_{\mathrm{FN}} = \hbar^2 k_{\mathrm{FN}}^2/2m$, and in the S layers $\mu - U(z) \equiv \varepsilon_{\mathrm{FS}} = \hbar^2 k_{\mathrm{FS}}^2/2m$. The solutions of Eq. (6) have to satisfy the periodicity condition

$$\begin{pmatrix} u(z+d) \\ v(z+d) \end{pmatrix} = e^{i\kappa d} \begin{pmatrix} u(z) \\ v(z) \end{pmatrix} \tag{8}$$

with the Bloch wave number κ.

For a multilayer with $\varepsilon_{\mathrm{FN}} = \varepsilon_{\mathrm{FS}} \equiv \hbar^2 k_F^2/2m$ the pair potential $\Delta(z)$ is given by the solid curve in Fig. 1. We define $k_{zF} = (k_F^2 - k_\varrho^2)^{1/2}$ and make the following WKBJ ansatz

$$\begin{pmatrix} u(z) \\ v(z) \end{pmatrix} \sim \begin{pmatrix} e^{i\eta(z)/2} \\ e^{-i\eta(z)/2} \end{pmatrix} e^{i\xi(z)} e^{ik_{zF} z} \tag{9}$$

where the slowly varying functions $\eta(z)$ and $\xi(z)$ have to satisfy[3,34]

$$\nabla_z \eta = \frac{2m}{\hbar^2 k_{zF}} [E - \Delta(z)\cos\eta], \tag{10a}$$

$$\nabla_z \xi = i\frac{m}{\hbar^2 k_{zF}} \Delta(z) \sin\eta. \tag{10b}$$

As has been shown in Refs. 3 and 34, these equations have two (linearly independent) solutions $\eta_1(z), \xi_1(z)$ and $\eta_2(z), \xi_2(z)$. Matching the linear combinations of the corresponding quasiparticle wave functions in $z = -a/2$ and observing Eq. (8) we obtain the eigenvalue equation

$$\begin{aligned} 0 = {} & 2\sin\{[\eta_2(-a/2) - \eta_1(-a/2)]/2\}\cos[(\kappa - k_{zF})d] - \exp\{-i[\xi_2(-a/2) - \xi_1(-a/2) + 2\xi_S]\}\sin\eta_1(-a/2) \\ & + \exp\{i[\xi_2(-a/2) - \xi_1(-a/2) + 2\xi_S]\}\sin\eta_2(-a/2). \end{aligned} \tag{11}$$

Here

$$\xi_S \equiv (m/\hbar^2 k_{zF})(E^2 - \Delta_0^2)^{1/2} b/2$$

for $E > \Delta(b/2) \equiv \Delta_0$, and

$$\xi_S \equiv i(m/\hbar^2 k_{zF})(\Delta_0^2 - E^2)^{1/2} b/2$$

for $E < \Delta_0$.

In order to compute the energy eigenvalues from Eq. (11) the differential Eqs. (10) are rewritten as integral equations [see Eqs. (7) and (8) of Ref. 34]. These equations are either integrated numerically subject to the boundary conditions

$$\eta_{1,2}(z = b/2) = \pm i\,\mathrm{arccosh}(E/\Delta_0), \tag{12a}$$

$$\xi_{1,2}(z = b/2) = \pm\frac{m}{\hbar^2 k_{zF}}(E^2 - \Delta_0^2)^{1/2} b/2 \tag{12b}$$

for $E > \Delta_0$ and

$$\eta_{1,2}(z = b/2) = \pm\arccos(E/\Delta_0), \tag{13a}$$

$$\xi_{1,2}(z = b/2) = \pm i\frac{m}{\hbar^2 k_{zF}}(\Delta_0^2 - E^2)^{1/2} b/2 \tag{13b}$$

for $E < \Delta_0$, or solved analytically in first-order Picard iteration as indicated in Ref. 34. The $\eta(E, k_{zF})$ and $\xi(E, k_{zF})$ obtained by either of the two procedures are inserted into the eigenvalue equation, Eq. (11), which is solved numerically. The results are shown in Figs. 3–6. We note that the spectra obtained from numerical integration and first-order Picard iteration agree very well. [As in SNS contacts,[34] the energy eigenvalue equation obtained by first-order Picard iteration with the self-consistent pair potential, solid curve in Fig. 1, is identical to that obtained with the periodic square-well potential, dashed curve in Fig. 1. It has the form of Eq. (21) with effective N- and S-layer thicknesses.] The good quantitative agreement of the results from the two methods indicates that the following approximate description of

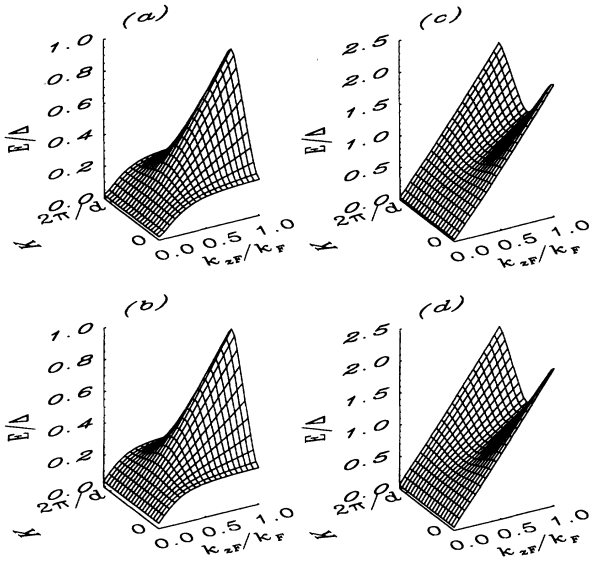

FIG. 3. Dispersion relation $E(k_{zF},\kappa)$ vs $k_{zF}=(k_F^2-k_\varrho^2)^{1/2}$ and $K\equiv k_{zF}-\kappa$ for the lowest (a),(b) and the next higher (c),(d) band of the multilayer of Fig. 1; (a),(c) for the square well and (b),(d) for the self-consistent pair potential; κ = Bloch wave number.

multilayers is sufficient: Replace the self-consistent pair potential $\Delta(z)$ by a periodic square well pair potential as shown in Fig. 1, where the area under both curves is equal, and assign the effective thickness

$$a_{\text{eff}}=2\int_{-a/2}^{b/2}[1-\Delta(z)/\Delta_0]\,dz \tag{14}$$

to the N layer with vanishing pair potential. The main error associated with this approximation is the slight difference[34] in the density of states for $E\to 0$ and a small reduction of bandwidths; see Figs. 4–6.

B. Localization effects

In the following we consider multilayers with $\varepsilon_{\text{FS}}\geq\varepsilon_{\text{FN}}$. They are described by Eqs. (6) where the pair potential is given by the dashed square-well form of Fig. 1. In addition to the periodicity condition, Eq. (8), matching of the quasiparticle wave functions $u(z)$ and $v(z)$ and of their derivatives at the N-S interfaces in $z=0$ and $z=-a$ is required. The wave functions and the derivation of the eigenvalue equation

$$D_0+D_1\theta+D_2\theta^2+D_1\theta^3+D_0\theta^4=0 \tag{15}$$

are given in the Appendix: $\theta=e^{i\kappa d}$. Equation (15) is valid for all energies E and absolute values k_ϱ of the wave vector parallel to the interfaces. The explicit form of $D_i=D_i(E,k_\varrho)$, $i=0,1,2$, is given in Eqs. (A12)–(A14). The functions D_0, D_1, and D_2 are all either purely real or purely imaginary so that they always can be redefined as real functions in the eigenvalue equation, Eq. (15). Multiplying Eq. (15) with θ^{*2}, and adding the equation thus obtained to the original one, results in a quadratic equation for $\cos(\kappa d)$, which has the two solutions

$$\begin{aligned}\cos\left(\kappa^{\pm}d\right)&=-\tilde{D}_1/4\pm\left[\left(\tilde{D}_1/4\right)^2-\tilde{D}_2/4+1/2\right]^{1/2}\\&\equiv F^{\pm}(E,k_\varrho)\\ \tilde{D}_1&\equiv D_1/D_0,\quad \tilde{D}_2\equiv D_2/D_0.\end{aligned} \tag{16}$$

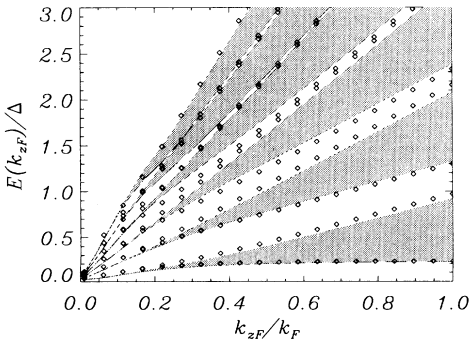

FIG. 4. Energy bands of the multilayer of Fig. 1. The diamonds indicate the band edges calculated with the self-consistent pair potential, whereas the shaded areas represent the bands computed with the square-well pair potential.

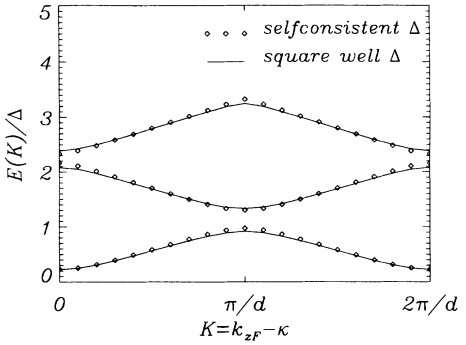

FIG. 5. Dispersion relation $E(K)$ of the three lowest bands of Fig. 4 at $k_{zF}=k_F$.

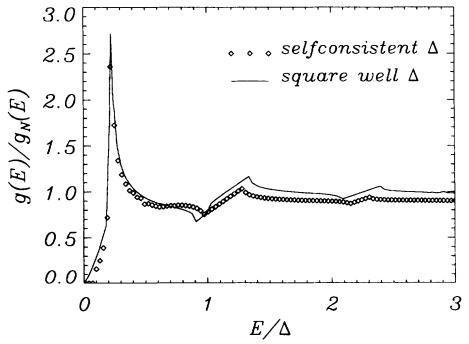

FIG. 6. The global density of states per unit area — normalized to $g_N(E)=2mdk_F/\pi^2\hbar^2$ — for the multilayer of Fig. 1. The peak at $E\approx 0.3\,\Delta$ corresponds to the lowest band edge at $k_{zF}=k_F$ in Figs. 3–5. There is no peak at $E=\Delta$ because the S layers are much thinner than the N layers.

This equation can be solved only for those values of E and k_ϱ for which

$$\left(\tilde{D}_1/4\right)^2 - \tilde{D}_2/4 + 1/2 \geq 0 \tag{17}$$

and

$$\left|F^{\pm}(E, k_\varrho)\right| \leq 1. \tag{18}$$

This results in the energy bands shown in Figs. 7 and 8. For the special case of equal Fermi energies in N and S layers, which are much larger than the pair potential, the eigenvalue equation can be further simplified. Observing $k_{z\mathrm{FS}}^2 = k_{z\mathrm{FN}}^2 = k_{zF}^2 \gg 2mE/\hbar^2$ one obtains

$$\tilde{D}_1 = -4Z\cos\left(k_{zF}d\right), \tag{19a}$$

$$\tilde{D}_2 = 2 + 4Z^2 - 4\sin^2\left(k_{zF}d\right) \tag{19b}$$

with

$$Z \equiv \cos(q\delta b)\cos(qa) - \delta^{-1}\sin(q\delta b)\sin(qa), \tag{20}$$

where $q = mE/\hbar^2 k_{zF}$ and $\delta = (1 - \Delta^2/E^2)^{1/2}$. This, inserted into Eq. (16), yields the well known eigenvalue equation[2–4]

$$\cos\left[\left(\kappa^{\pm} \pm k_{zF}\right)d\right] = Z. \tag{21}$$

This equation is also valid in the first-order Picard iteration of the WKBJ approximation for self-consistent pair potentials as indicated in Sec. III A. κ^+ refers to the upper and κ^- to the lower sign in Eq. (21). The corresponding energy bands are shown in Fig. 9. In Figs. 7 and 9 the Bloch bands degenerate into discrete levels for small energies and small $k_{z\mathrm{FN}} = (k_{\mathrm{FN}}^2 - k_\varrho^2)^{1/2}$. This is a consequence of quasiparticle localization in the N layers because of nearly perfect Andreev scattering.

In Fig. 8 we observe that in the case $\varepsilon_{\mathrm{FS}} > \varepsilon_{\mathrm{FN}}$ the spatially varying scalar potential $U(z)$ removes the degeneracy at $\kappa d = n\pi$, n = integer, one has in the case $\varepsilon_{\mathrm{FN}} = \varepsilon_{\mathrm{FS}}$. For smaller k_{zF} the band-edge separation becomes larger and results in the "band holes" and the band splitting one notes in Fig. 7.

From the solutions of the eigenvalue equation, Eq. (16), the global density of states per unit area of the cross

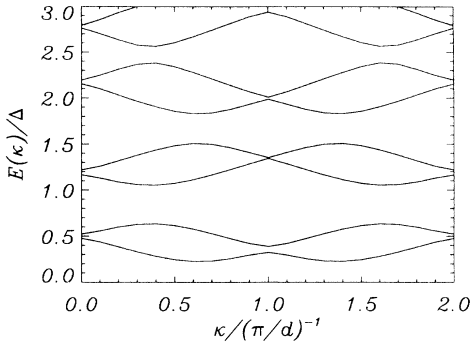

FIG. 8. Band structure of the energy bands of Fig. 7 at $k_{z\mathrm{FN}}/k_{\mathrm{FN}} = 1$.

section $L_x L_y$ is calculated for both spin orientations in a periodicity volume of length d according to

$$\begin{aligned} g(E) &= \frac{1}{L_x L_y}\sum_{\mathbf{k}_\varrho,\kappa}\delta\left(E - E\left(k_\varrho,\kappa\right)\right) \\ &= \frac{1}{\pi}\int dk_\varrho\, k_\varrho \sum_{i=+,-}\frac{d}{\pi}\int d\kappa^i \delta\left(E - E\left(k_\varrho,\kappa^i\right)\right) \\ &= \frac{d}{\pi^2}\int dk_\varrho\, k_\varrho \sum_{i=+,-}\left|\frac{\partial\kappa^i}{\partial E(k_\varrho,\kappa^i)}\right|_{E(k_\varrho,\kappa^i)=E}. \end{aligned} \tag{22}$$

From Eq. (16) we see, that

$$\left|\frac{\partial\kappa^i}{\partial E(k_\varrho,\kappa^i)}\right| = \frac{1}{d}\left|\frac{\partial \arccos\left[F^i(E,k_\varrho)\right]}{\partial E}\right|. \tag{23}$$

Integration over k_ϱ is limited to the intervals where Eqs. (17) and (18) are satisfied. For fixed E these intervals can be read off from Figs. 7 and 9: They are given by the cuts of the straight line E = const with the curves, which limit the energy bands indicated by the shaded areas. The energy eigenvalues of those states, which are localized in the S layer because of the k_ϱ mismatch and of those localized in the N layer because their S-layer penetration depth is much less than b, are independent of κ. They contribute to the density of states like the corresponding (E, k_ϱ) states in isolated superconducting films of thickness b, and SNS junctions of N-layer thickness a

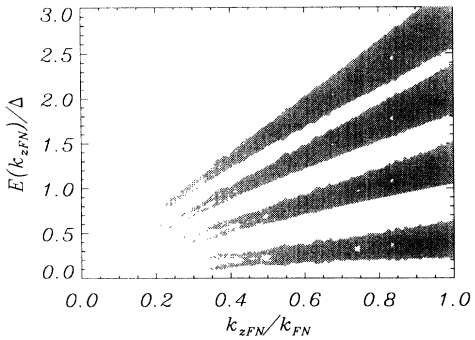

FIG. 7. Energy bands of a multilayer: $a = 8\,\xi_0$, $b = 3\,\xi_0$, $\varepsilon_{\mathrm{FS}}/\varepsilon_{\mathrm{FN}} = 4/3$, $\varepsilon_{\mathrm{FS}}/\Delta = 5000$, $T = 0.5\,T_C$.

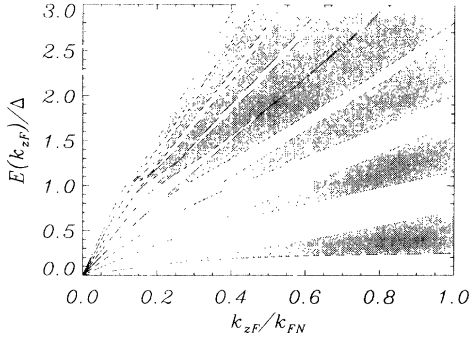

FIG. 9. Energy bands of a multilayer with $\varepsilon_{\mathrm{FS}} = \varepsilon_{\mathrm{FN}}$; otherwise same parameters as in Fig. 7.

and semi-infinite S banks, respectively. The k_ϱ mismatch results in an imaginary $k_{z\mathrm{FN}}$, according to Eq. (A7), and thus an exponential damping of the quasiparticle wave functions in the N layer.

Some typical examples of global density of states curves are shown in Figs. 10 and 11. For thick S banks and $\varepsilon_{\mathrm{FS}} = \varepsilon_{\mathrm{FN}}$ the density of states curve in Fig. 10 exhibits the subgap peak, the BCS peak and the Tomasch-McMillan-Anderson oscillations one knows from SNS contacts.[34,36] With increasing ratio $\varepsilon_{\mathrm{FS}}/\varepsilon_{\mathrm{FN}}$ the subgap peak decreases and the BCS peak becomes more pronounced. This is the consequence of the increasing number of states localized in the S layers. In multilayers with thinner S layers, Fig. 11, the subgap peak is more pronounced and splits in two for $\varepsilon_{\mathrm{FS}} = 2\varepsilon_{\mathrm{FN}}$. This is associated with the band splitting discussed in the context of Figs. 7 and 8. Also the effect of the Tomasch-McMillan-Anderson oscillations becomes more dramatic in the vicinity of $E \geq \Delta$. Figure 12 exhibits the variation of the density of states with temperature. The temperature variation of the energetic position of the subgap peak relative to $\Delta(T)$, i.e., the position of the BCS peak of a homogeneous superconductor, is also indicated in Fig. 13 for two multilayers and one SNS junction. In the temperature range not too close to T_C this position shows a slower decrease with temperature than $\Delta(T)$, and this effect becomes more pronounced with increasing probability of finding quasiparticles in the S layers, i.e., with increasing $\varepsilon_{\mathrm{FS}}/\varepsilon_{\mathrm{FN}}$. This in turn is consistent with the even slower decrease of the subgap peak position in the SNS junction ($b \to \infty$). In HTSC one has experimentally found energy gaps, normalized to their $T = 0\,\mathrm{K}$ value, considerably above the BCS curve $\Delta(T)/\Delta(T = 0\,\mathrm{K})$.[22,24] It remains to be seen whether this has something to do with the subgap peak temperature dependence of our simple multilayer model.

The local density of states is given by the one-particle spectral function in the quasiparticle approximation[5,37]

$$\rho(E,z) = \sum_i \left[|u_i(z)|^2 \, \delta(E - E_i) + |v_i(z)|^2 \, \delta(E + E_i) \right], \tag{24}$$

where the summation over $i = (\mathbf{k}_\varrho, \kappa)$ is restricted to

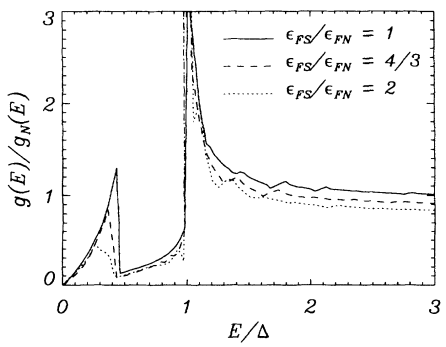

FIG. 10. Global densities of states for multilayers with thick superconducting layers, $a = 8\,\xi_0$, $b = 18\,\xi_0$, and different Fermi-energy ratios.

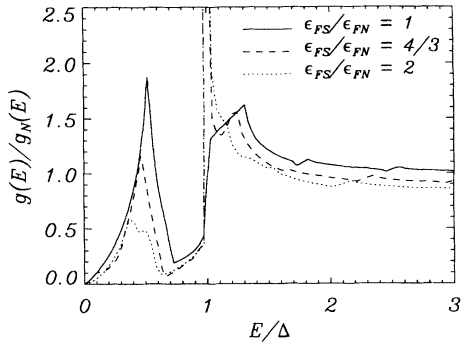

FIG. 11. Global densities of states for multilayers with $a = 5\,\xi_0$, $b = 8\,\xi_0$ and different Fermi-energy ratios.

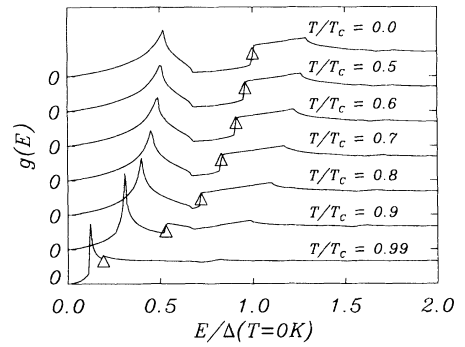

FIG. 12. Temperature dependence of the global density of states of a multilayer with $a = 5\,\xi_0$, $b = 8\,\xi_0$, and $\varepsilon_{\mathrm{FS}} = \varepsilon_{\mathrm{FN}}$. The triangles mark the energetic positions of the BCS peak of a homogeneous superconductor.

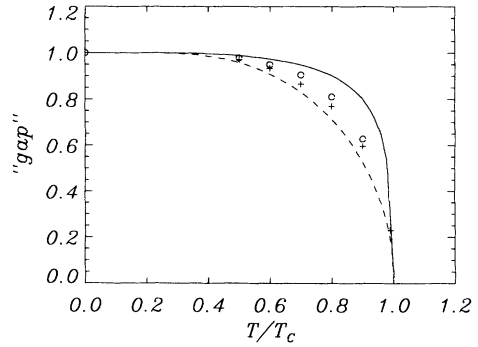

FIG. 13. Temperature dependence of the energetic position of the subgap peak, normalized to the position at $T = 0\,\mathrm{K}$, for a multilayer with $a = 5\,\xi_0$, $b = 8\,\xi_0$ and $\varepsilon_{\mathrm{FS}}/\varepsilon_{\mathrm{FN}} = 1.0$ (+), and $\varepsilon_{\mathrm{FS}}/\varepsilon_{\mathrm{FN}} = 2.0$ (o). Also shown is this temperature dependence for an SNS junction ($b \to \infty$) with $\varepsilon_{\mathrm{FS}}/\varepsilon_{\mathrm{FN}} = 1.0$ and N layer thickness $a = 6\,\xi_0$: solid line. For comparison the BCS temperature dependence of the pair potential of a bulk superconductor is indicated by the dashed line.

positive energy states.[38] Combining Eqs. (A8) and (A11) with the analytically evaluated normalization condition

$$\int \left[|u|^2 + |v|^2\right] d^3r = 1 \tag{25}$$

results in a system of equations from which the coefficients $A_1, \ldots, A_8$ are determined numerically. Thus, the quasiparticle wave functions u and v required for the numerical computation of the local density of states according to Eq. (24) are known completely. Comparison of Fig. 14 with Fig. 15 shows that the increase in the density of states at $E = \Delta$ associated with the increase of $\varepsilon_{FS}/\varepsilon_{FN}$ occurs in the superconducting layer $0 < z < b/2$ indeed, as a consequence of the increasing localization of quasiparticles in this region. The subgap peak of Fig. 14 decreases as one goes from N to S, and a small energy gap opens up in S as can be noted from the dashed curve in Fig. 16. Our multilayer densities of states, which take into account all states, even the ones that hardly feel the superconducting layers at all because $k_\varrho \to k_{FN}$, do not contain an N-side energy gap as was obtained by Hara, Ashida, and Nagai[35] for double layers.

In the numerical computation of the energy bands and densities of states presented so far we have chosen $\Delta/\varepsilon_{FS,N} < 2 \times 10^{-4}$. With the view at the HTSC, the energy bands and densities of states presented in Figs. 17–20 have been computed for much larger ratios, i.e., $\Delta/\varepsilon_{FS} = 10^{-2}$ and $\Delta/\varepsilon_{FN} = 1$. In Fig. 17 the band structure of the lowest subband, i.e., the dependence of the energy on k_{zFN} and the Bloch wave number κ, is shown explicitly. The oscillations of the subband energies as functions of k_{zFN} shown in Fig. 18 are similar to the oscillations of the energy eigenvalues of superconducting–semiconducting–superconducting (S-Sem-S) junctions.[27,39] Nevertheless, there are two basic differences in the energy spectra of multilayers with $\varepsilon_{FS} \gg \varepsilon_{FN}$ and S-Sem-S junctions: The additional κ dependence in the multilayers, indicated by the shaded areas in Fig. 18, and the discrete, finite energies of quasiparticles moving parallel to the interface in S-Sem-S junctions with their different effective masses;[27,39] these energies approach zero in our multilayers with constant effective masses. The local and the global densities of states of Figs. 19 and 20 are practically that of a bulk superconductor for $E \geq \Delta$. The reason is that the electron density is much higher in the S than in the N layers,

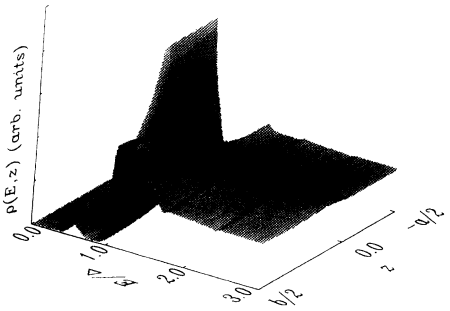

FIG. 14. Local density of states $\rho(E, z)$ of a multilayer with $\varepsilon_{FS}/\varepsilon_{FN} = 1$, otherwise the same parameters as in Fig. 11.

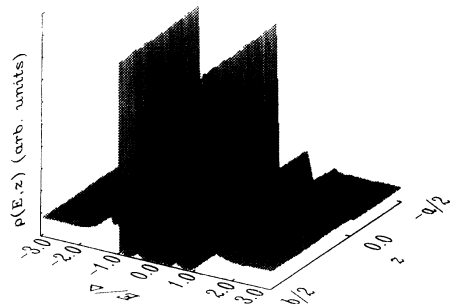

FIG. 15. Local density of states of a multilayer with $\varepsilon_{FS}/\varepsilon_{FN} = 4/3$, otherwise same parameters as in Fig. 14.

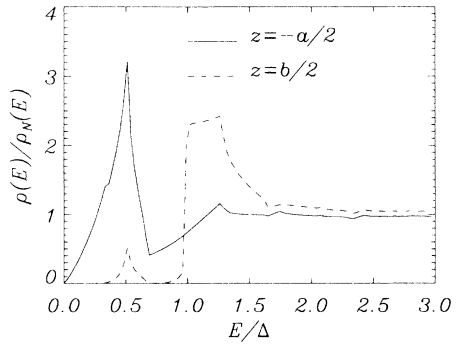

FIG. 16. Cuts of $\rho(E, z)$ in Fig. 14 with the planes $z = -a/2$ and $z = b/2$; $\rho_N(E)$ = local density of states of the multilayer at $T > T_{CS}$. There is excellent qualitative agreement with the local density of states computed by Tanaka and Tsukada[5] from a combination of solutions of the BdGE and the Gorkov equations.

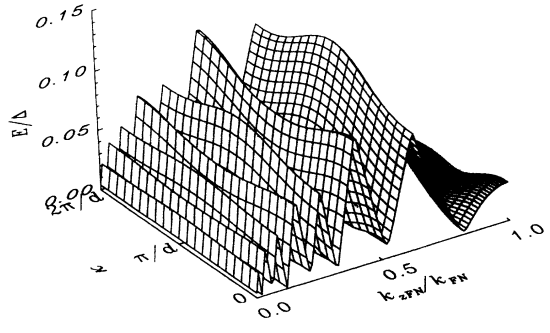

FIG. 17. Lowest-energy band $E(k_{zFN}, \kappa)$ of a multilayer with $a = 4\xi_0$, $b = 1\xi_0$, $\varepsilon_{FS}/\varepsilon_{FN} = 100$, $\varepsilon_{FS}/\Delta = 100$, at $T = 0$ K.

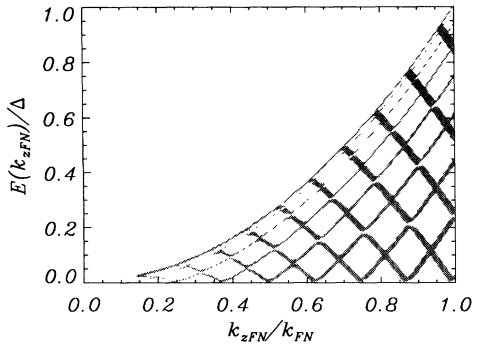

FIG. 18. Energy bands of the multilayer with the parameters of Fig. 17 ($k_{FN} = 0.1\,k_{FS}$).

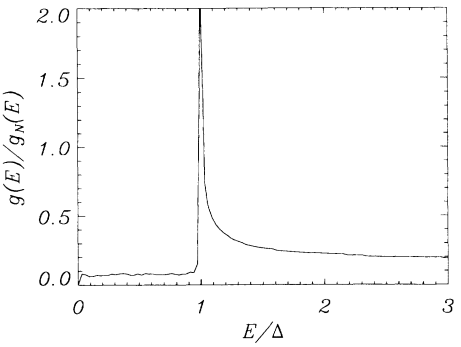

FIG. 20. Global density of states of the multilayer with the parameters of Fig. 17.

and the severe mismatch for nearly all but the smallest k_ϱ inhibits the penetration of the overwhelming majority of S layer electrons into the N layers. There remains a nearly constant small density of states for $E < \Delta$, which is localized in the N layers and drops to zero close to $E = 0$. The approach of the multilayer density of states to the BCS density of states for $E \geq \Delta$ with increasing ratio $\varepsilon_{FS}/\varepsilon_{FN}$ can also be noted from Fig. 11.

IV. DISCUSSION

We have shown that the energy bands and the densities of states of multilayers computed with self-consistent pair potentials on the one hand and their equivalent square-well representations on the other hand show very little difference. They exhibit features already known from SNS junctions, such as the subgap peak and the Tomasch-McMillan-Anderson oscillations in the density of states, which are due to off-diagonal (Andreev) scattering and interference between electron and hole waves.[34] If the thickness of the superconducting layers exceeds many coherence lengths one has quasiparticle localization in the N layers for energies below the maximum value of the pair potential Δ because of Andreev scattering. With decreasing S-layer thickness Bloch wave propagation removes this localization. In multilayers where the Fermi energy in the S layers is larger than that in the N layers one has additional localization in the S and the N layers because of diagonal (electron-electron and hole-hole) scattering. In this case the mismatch of the wave vectors parallel to the interfaces (k_ϱ mismatch) inhibits Bloch wave propagation of S-layer electrons.

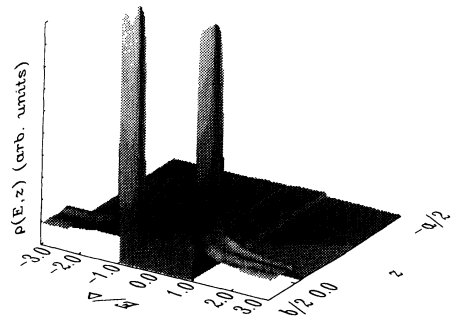

FIG. 19. Local density of states of the multilayer with the parameters of Fig. 17. The qualitative aspects, namely, a metalliclike density of states in the N and BCS-like density of states in the S layers, do not change if ε_{FN} is increased up to about $10\,\Delta$.

Most detailed information on the electronic structure of multilayers is given by the local densities of states, such as the ones shown in Figs. 14–16 and 19. They can be measured experimentally by the method of scanning tunneling microscopy (STM) applied by Tanaka *et al.*[20] to the bulk single grain high-T_C superconductor $YBa_2Cu_3O_7$. These authors find periodic alternating BCS-like and metalliclike STM conductance spectra. The local density of states of Fig. 19 is BCS-like in the S and metalliclike in the N layers, indeed. This seems to indicate that the findings from our multilayer theory (which is based on Fermi-liquid quasiparticles and Gorkov pairing interaction[40,41]) may have some relevance for the understanding of the electronic structure of HTSC, despite of the many open questions concerning the normal and superconducting state of the HTSC, such as the applicability of Fermi-liquid theory and the nature of the pairing mechanism.

In other HTSC like $Bi_2Sr_2CaCu_2O_{8+\delta}$ two energy gaps have been measured,[22,23] one of which has a ratio $2\Delta(0)/k_BT_C$ considerably larger than the BCS value. These gaps decrease more slowly with temperature in temperature ranges not too close to T_C than the gap of BCS theory.[22] Slow gap variations with temperature have also been observed in $Y_{0.5}Sm_{0.5}Ba_2Cu_3O_{7-\delta}$, $DyBa_2Cu_3O_{7-\delta}$, $Bi_2Sr_2CaCu_2O_{8-y}$,[24] and $Bi_2Sr_2CaCu_2O_8$.[21] The subgap peak in the global density of states, present in multilayers and SNS junctions (in addition to the BCS peak), shows a similar temperature dependence; see Fig. 13. However, in the experiments of Refs. 22 and 23 the weaker temperature dependence is associated with the larger of the two gaps, both of which are related to the anisotropy of $Bi_2Sr_2CaCu_2O_{8+\delta}$.

In our multilayer model anisotropic pairing interactions have not been taken into account. However, we have seen that in the energy range $E \geq \Delta$ the density of states of multilayers with even very thin S layers approaches that of a bulk BCS superconductor with increas-

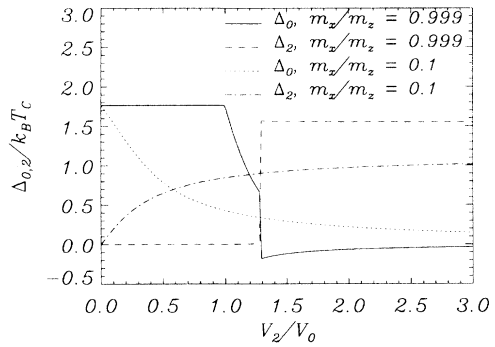

FIG. 21. Isotropic (Δ_0) and anisotropic (Δ_2) component of the pair potential of a bulk superconductor vs the ratio V_2/V_0 between anisotropic and isotropic pairing interaction for two different effective mass ratios.

ing Fermi energy ratio $\varepsilon_{\mathrm{FS}}/\varepsilon_{\mathrm{FN}}$ because of increasing localization of quasiparticles in the S layers due to the k_ϱ mismatch. Therefore it might not be completely unjustified to expect that in the energy range $E \geq \Delta$ multilayers with $\varepsilon_{\mathrm{FS}} \gg \varepsilon_{\mathrm{FN}}$ and with anisotropic pairing interactions exhibit the total density of states of a bulk superconductor with anisotropic pairing interaction. This density of states has been computed by us[42] taking into account a Legendre polynomial superposition of s- and d-wave pairing interaction,[31] and an anisotropic effective mass with $m_x = m_y < m_z$. A solution of the appropriately modified BCS gap equation[42] is found with the ansatz

$$\Delta(\hat{\mathbf{k}}) = \Delta_0 + \Delta_2(2\hat{k}_z^2 - \hat{k}_x^2 - \hat{k}_y^2), \tag{26}$$

which consists of the superposition of an isotropic (s-) wave part Δ_0 and an anisotropic (d-) wave part Δ_2.[31] $\hat{k}_i$, $i = x, y, z$ is the ith component of the unit vector $\hat{\mathbf{k}}$. The solutions for Δ_0 and Δ_2 at $T = 0.1\,T_C$ are shown in Fig. 21. The density of states $g(E)$ in the case of strong anisotropy, Fig. 22, exhibits two peaks, the relative magnitude of which varies with the ratio of the effective mass components. One is at $E \approx 1.6\,k_BT_C$ and the other one is above. Thus, anisotropy may indeed account for two density of states peaks in superconducting multilayers. However, $|\Delta(\hat{k} = \hat{k}_z)| > |\Delta(\hat{k}_z = 0)|$, whereas the experimental findings in HTSC indicate the opposite.[22,23]

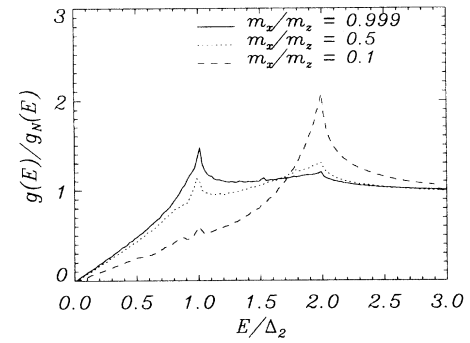

FIG. 22. Densities of states of anisotropic bulk superconductors with different effective mass ratios and large V_2/V_0 normalized to the density of states in the normal state.

Thus, as in the phenomenon of the subgap peak and BCS peak, further theoretical and experimental research will be necessary in order to clarify if these double peaks are related to the experimentally found two energy gaps in the above-mentioned HTSC. Appropriate theoretical methods to be used in future studies of strongly correlated, inhomogeneous superconducting systems are the stationary[43] and time-dependent[42,44] density functional Bogoliubov–de Gennes equations.

ACKNOWLEDGMENTS

The authors are grateful for support by the Deutsche Forschungsgemeinschaft and the Rechenzentrum der Universität Würzburg.

APPENDIX: QUASIPARTICLE WAVE FUNCTIONS AND EIGENVALUE EQUATION

In the superconducting layer $0 < z < b$ the solutions of the BdGE, Eq. (6), with the periodic square-well pair potential of Fig. 1 are

$$\begin{pmatrix} u(z) \\ v(z) \end{pmatrix} = A_1 \begin{pmatrix} \Gamma^+ \\ \Gamma^- \end{pmatrix} \sin\left(k_S^+ z\right) + A_2 \begin{pmatrix} \Gamma^+ \\ \Gamma^- \end{pmatrix} \cos\left(k_S^+ z\right) + A_3 \begin{pmatrix} \Gamma^- \\ \Gamma^+ \end{pmatrix} \sin\left(k_S^- z\right) + A_4 \begin{pmatrix} \Gamma^- \\ \Gamma^+ \end{pmatrix} \cos\left(k_S^- z\right), \tag{A1}$$

where for $E \geq \Delta$

$$k_S^\pm = \left[k_{z\mathrm{FS}}^2 \pm \left(2mE/\hbar^2\right)\delta\right]^{1/2}, \tag{A2}$$

$$k_{z\mathrm{FS}} \equiv (2m\varepsilon_{\mathrm{FS}}/\hbar^2 - k_\varrho^2)^{1/2}, \tag{A3}$$

and

$$\delta \equiv (1 - \Delta^2/E^2)^{1/2}. \tag{A4}$$

The spinor components are $\Gamma^\pm = (1 \pm \delta)^{1/2}$. For $E < \Delta$, with δ purely imaginary, $\Gamma^\pm$ and the wave numbers $k_S^\pm$ are complex. The quasiparticle wave functions in the normal layer are given by

$$\begin{pmatrix} u(z) \\ v(z) \end{pmatrix} = A_5 \begin{pmatrix} 1 \\ 0 \end{pmatrix} \sin\left(k_N^+ z\right) + A_6 \begin{pmatrix} 1 \\ 0 \end{pmatrix} \cos\left(k_N^+ z\right) + A_7 \begin{pmatrix} 0 \\ 1 \end{pmatrix} \sin\left(k_N^- z\right) + A_8 \begin{pmatrix} 0 \\ 1 \end{pmatrix} \cos\left(k_N^- z\right), \tag{A5}$$

where

$$k_N^\pm = (k_{z\mathrm{FN}}^2 \pm 2mE/\hbar^2)^{1/2}, \tag{A6}$$

$$k_{z\mathrm{FN}} \equiv (2m\varepsilon_{\mathrm{FN}}/\hbar^2 - k_\varrho^2)^{1/2}. \tag{A7}$$

The matching and the periodicity conditions result in the linear homogeneous system of equations

$$\check{M} \cdot \mathbf{A} = \mathbf{0} \tag{A8}$$

for the vector $\mathbf{A}$ of the coefficients $A_1, \ldots, A_8$ with the 8×8 matrix

$$\check{M} = \begin{pmatrix} 0 & \Gamma^+ & 0 & \Gamma^- & 0 & 1 & 0 & 0 \\ 0 & \Gamma^- & 0 & \Gamma^+ & 0 & 0 & 0 & 1 \\ k_S^+\Gamma^+ & 0 & k_S^-\Gamma^- & 0 & k_N^+ & 0 & 0 & 0 \\ k_S^+\Gamma^- & 0 & k_S^-\Gamma^+ & 0 & 0 & 0 & k_N^- & 0 \\ \Gamma^+ s_3 & \Gamma^+ c_3 & \Gamma^- s_4 & \Gamma^- c_4 & -\theta s_1 & \theta c_1 & 0 & 0 \\ \Gamma^- s_3 & \Gamma^- c_3 & \Gamma^+ s_4 & \Gamma^+ c_4 & 0 & 0 & -\theta s_2 & \theta c_2 \\ k_S^+\Gamma^+ c_3 & -k_S^+\Gamma^+ s_3 & k_S^-\Gamma^- c_4 & -k_S^-\Gamma^- s_4 & \theta k_N^+ c_1 & \theta k_N^+ s_1 & 0 & 0 \\ k_S^+\Gamma^- c_3 & -k_S^+\Gamma^- s_3 & k_S^-\Gamma^+ c_4 & -k_S^-\Gamma^+ s_4 & 0 & 0 & \theta k_N^- c_2 & \theta k_N^- s_2 \end{pmatrix}. \tag{A9}$$

Here $\theta = e^{i\kappa d}$ and

$$\begin{aligned} s_1 &\equiv \sin\left(k_N^+ a\right), & c_1 &\equiv \cos\left(k_N^+ a\right), \\ s_2 &\equiv \sin\left(k_N^- a\right), & c_2 &\equiv \cos\left(k_N^- a\right), \\ s_3 &\equiv \sin\left(k_S^+ b\right), & c_3 &\equiv \cos\left(k_S^+ b\right), \\ s_4 &\equiv \sin\left(k_S^- b\right), & c_4 &\equiv \cos\left(k_S^- b\right). \end{aligned} \tag{A10}$$

The requirement $\mathrm{Det}\check{M} = 0$ yields the eigenvalue equation of the system, which can be brought in the form

$$D_0 + D_1\theta + D_2\theta^2 + D_1\theta^3 + D_0\theta^4 = 0. \tag{A11}$$

Here D_0, D_1, and D_2 are subdeterminants or linear combinations of subdeterminants. They depend on the quasiparticle energy E and the absolute value of the wave vector $\mathbf{k}_\varrho$ parallel to the interfaces. They have been determined with the help of the computer algebra program MATHEMATICA:

$$D_0 = 4\delta^2 k_N^+ k_N^- k_S^+ k_S^-, \tag{A12}$$

$$\begin{aligned} D_1 = & -4\delta k_N^+ k_N^- k_S^+ k_S^- \left\{c_1\left[c_4(\delta-1)+c_3(\delta+1)\right]+c_2\left[c_3(\delta-1)+c_4(\delta+1)\right]\right\} \\ & + 2\delta k_N^- k_S^+ k_S^- s_1\left[k_S^+ s_3(\delta+1)+k_S^- s_4(\delta-1)\right] + 2\delta k_N^+ k_S^+ k_S^- s_2\left[k_S^+ s_3(\delta-1)+k_S^- s_4(\delta+1)\right] \\ & + 2\delta k_N^{+2} k_N^- s_1\left[k_S^+ s_4(\delta-1)+k_S^- s_3(\delta+1)\right] + 2\delta k_N^+ k_N^{-2} s_2\left[k_S^+ s_4(\delta+1)+k_S^- s_3(\delta-1)\right], \end{aligned} \tag{A13}$$

$$\begin{aligned} D_2 = & \ 4\,\delta^2 s_1 s_2 s_3 s_4 (k_N^{+2} k_N^{-2} + k_S^{+2} k_S^{-2}) - 4\delta k_N^- k_S^+ k_S^- s_1 c_2\left[k_S^+ s_3 c_4(\delta+1)+k_S^- c_3 s_4(\delta-1)\right] \\ & - 4\delta k_N^+ k_S^+ k_S^- c_1 s_2\left[k_S^+ s_3 c_4(\delta-1)+k_S^- c_3 s_4(\delta+1)\right] - 4\delta k_N^{+2} k_N^- s_1 c_2\left[k_S^- s_3 c_4(\delta+1)+k_S^+ c_3 s_4(\delta-1)\right] \\ & - 4\delta k_N^+ k_N^{-2} c_1 s_2\left[k_S^- s_3 c_4(\delta-1)+k_S^+ c_3 s_4(\delta+1)\right] \\ & + k_N^+ k_N^- c_1 c_2\left\{4k_S^+ k_S^-\left[(\delta^2-1)+c_3 c_4(3\delta^2+1)\right]+2s_3 s_4(1-\delta^2)(k_S^{+2}+k_S^{-2})\right\} \\ & + k_N^{+2} s_1 s_2\left\{2k_S^+ k_S^-\left[(\delta^2-1)+c_3 c_4(1-\delta^2)\right]+s_3 s_4\left[k_S^{+2}(1-\delta)^2+k_S^{-2}(1+\delta)^2\right]\right\} \\ & + k_N^{-2} s_1 s_2\left\{2k_S^+ k_S^-\left[(\delta^2-1)+c_3 c_4(1-\delta^2)\right]+s_3 s_4\left[k_S^{+2}(1+\delta)^2+k_S^{-2}(1-\delta)^2\right]\right\} \\ & + k_N^+ k_N^-\left\{4k_S^+ k_S^-\left[(\delta^2+1)+c_3 c_4(\delta^2-1)\right]+2s_3 s_4(\delta^2-1)(k_S^{+2}+k_S^{-2})\right\}. \end{aligned} \tag{A14}$$

Note that the trigonometric functions of Eq. (A10) have generally complex arguments.

[1] A. F. Andreev, Zh. Eksp. Teor. Fiz. **46**, 1823 (1964) [Sov. Phys. JETP **19**, 1228 (1964)].
[2] A. P. van Gelder, Phys. Rev. **181**, 787 (1969).
[3] R. Kümmel, Phys. Rev. B **3**, 784 (1971).
[4] A. Hahn, Physica B **165&166**, 1065 (1990).
[5] Y. Tanaka and M. Tsukada, Phys. Rev. B **44**, 7578 (1991).
[6] I. K. Schuller, Phys. Rev. Lett. **44**, 1597 (1980).
[7] K. Kanoda *et al.*, Phys. Rev. B **33**, 2052 (1986).
[8] H. C. Yang, C. H. Nien, H. H. Sung, and C. H. Chen, J. Low Temp. Phys. **75**, 243 (1989).
[9] S. T. Ruggiero, T. W. Barbee, and M. R. Beasley, Phys. Rev. Lett. **45**, 1299 (1980).
[10] S. N. Song, B. Y. Jin, F. L. Du, and J. B. Ketterson, Superlatt. Microstruct. **3**, 485 (1987), and references therein.
[11] H. Tabata, T. Kawai, and S. Kawai, Appl. Phys. Lett. **58**, 1443 (1991).
[12] T. Kawai *et al.*, Physica C **185-189**, 198 (1991).
[13] H. Tabata, T. Kawai, and S. Kawai, Phys. Rev. Lett. **70**, 2633 (1993).
[14] R. Li *et al.*, Phys. Rev. Lett. **70**, 3804 (1993).
[15] P. de Rango *et al.*, J. Phys. (Paris) **50**, 2857 (1989).
[16] J. R. Clem, in *Transport Properties of Superconductors*, edited by R. Nicolsky (World Scientific, Singapore, 1990), pp. 64–84.
[17] J. R. Clem and M. W. Coffey, Phys. Rev. B **42**, 6209 (1990).

[18] G. Deutscher, in *Transport Properties of Superconductors*, edited by R. Nicolsky (World Scientific, Singapore, 1990), pp. 2–10.
[19] S. Schreyer and K. Scharnberg, Verhandl. DPG (VI) **27**, 958 (1992); S. Schreyer, Diploma thesis, Universität Hamburg, 1993.
[20] M. Tanaka *et al.*, Jpn. J. Appl. Phys. **32**, 35 (1993).
[21] L. C. Brunel *et al.*, Phys. Rev. Lett. **66**, 1346 (1991).
[22] M. Boekholt, M. Hoffmann, and G. Güntherodt, Physica C **175**, 127 (1991).
[23] L. Buschmann, M. Boekholt, and G. Güntherodt, Physica C **203**, 68 (1992).
[24] A. M. Rao *et al.*, Phys. Rev. B **42**, 193 (1990).
[25] E. Polturak, G. Koren, D. Cohen, and E. Aharoni, Phys. Rev. B **47**, 5270 (1993).
[26] M. Y. Kupriyanov, Fiz. Nizk. Temp. **7**, 700 (1981) [Sov. J. Low Temp. Phys. **7**, 342 (1981)].
[27] U. Schüssler and R. Kümmel, Phys. Rev. B **47**, 2754 (1993).
[28] G. Kieselmann, Phys. Rev. B **35**, 6762 (1987).
[29] M. Ashida, S. Aoyama, J. Hara, and K. Nagai, Phys. Rev. B **40**, 8673 (1989).
[30] M. Ashida, J. Hara, and K. Nagai, Phys. Rev. B **45**, 828 (1992).
[31] C. Bruder, Phys. Rev. B **41**, 4017 (1990).
[32] A. V. Zaitsev, Zh. Eksp. Teor. Fiz. **86**, 1742 (1984) [Sov. Phys. JETP **59**, 1015 (1984)].
[33] J. Bardeen, R. Kümmel, A. E. Jacobs, and L. Tewordt, Phys. Rev. **187**, 556 (1969).
[34] H. Plehn, U. Gunsenheimer, and R. Kümmel, J. Low Temp. Phys. **83**, 71 (1991).
[35] J. Hara, M. Ashida, and K. Nagai, Phys. Rev. B **47**, 11 263 (1993).
[36] R. Kümmel, U. Schüssler, U. Gunsenheimer, and H. Plehn, Physica C **185-189**, 221 (1991).
[37] F. Gygi and M. Schlüter, Phys. Rev. B **43**, 7609 (1991).
[38] J. D. Shore, M. Huang, A. T. Dorsey, and J. P. Sethna, Phys. Rev. Lett. **62**, 3089 (1989).
[39] U. Gunsenheimer, U. Schüssler, and R. Kümmel, Phys. Rev. B **49**, 6111 (1994).
[40] P. G. deGennes, *Superconductivity of Metals and Alloys* (Benjamin, New York, 1966).
[41] A. A. Abrikosov, L. P. Gorkov, and I. E. Dzyaloshinski, *Methods of Quantum Field Theory in Statistical Physics* (Dover, New York, 1963).
[42] O.-J. Wacker, Ph.D. thesis, Universität Würzburg, 1993.
[43] L. N. Oliveira, E. K. U. Gross, and W. Kohn, Phys. Rev. Lett. **60**, 2430 (1988).
[44] O.-J. Wacker, R. Kümmel, and E. K. U. Gross (unpublished).

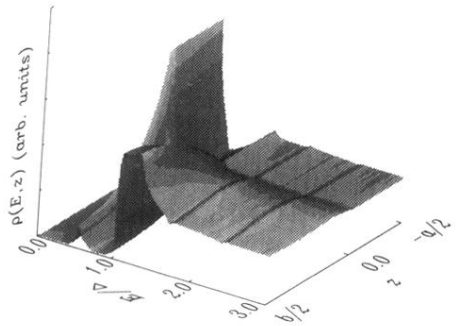

FIG. 14. Local density of states $\rho(E, z)$ of a multilayer with $\varepsilon_{\mathrm{FS}}/\varepsilon_{\mathrm{FN}} = 1$, otherwise the same parameters as in Fig. 11.

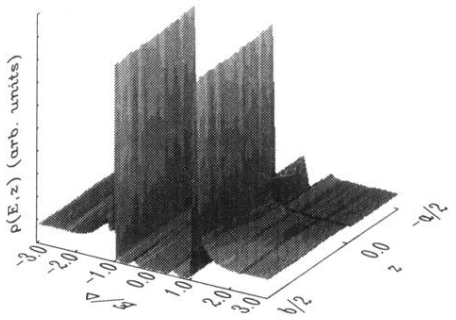

FIG. 15. Local density of states of a multilayer with $\varepsilon_{FS}/\varepsilon_{FN} = 4/3$, otherwise same parameters as in Fig. 14.

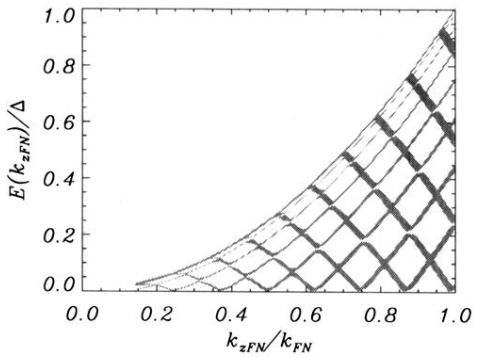

FIG. 18. Energy bands of the multilayer with the parameters of Fig. 17 ($k_{FN} = 0.1\, k_{FS}$).

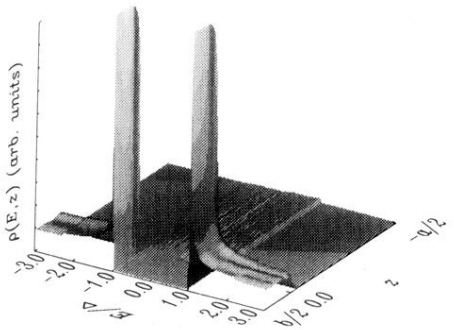

FIG. 19. Local density of states of the multilayer with the parameters of Fig. 17. The qualitative aspects, namely, a metalliclike density of states in the N and BCS-like density of states in the S layers, do not change if ϵ_{FN} is increased up to about $10\,\Delta$.

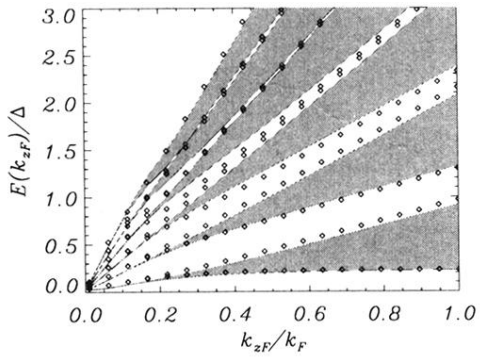

FIG. 4. Energy bands of the multilayer of Fig. 1. The diamonds indicate the band edges calculated with the self-consistent pair potential, whereas the shaded areas represent the bands computed with the square-well pair potential.

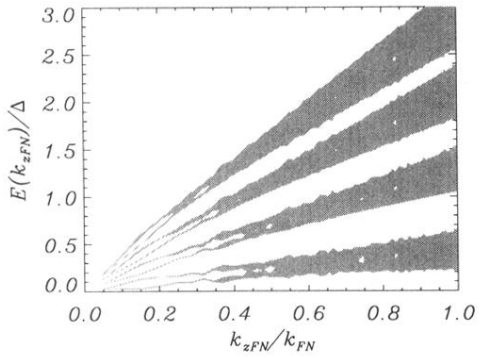

FIG. 7. Energy bands of a multilayer: $a = 8\,\xi_0$, $b = 3\,\xi_0$, $\varepsilon_{FS}/\varepsilon_{FN} = 4/3$, $\varepsilon_{FS}/\Delta = 5000$, $T = 0.5\,T_C$.

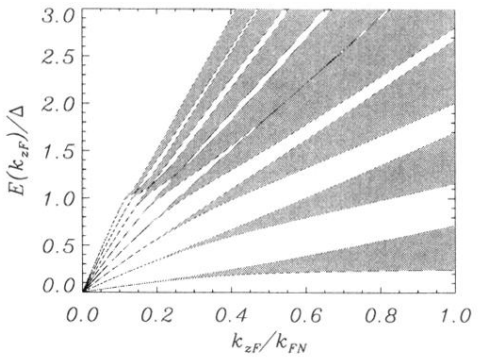

FIG. 9. Energy bands of a multilayer with $\varepsilon_{\mathrm{FS}} = \varepsilon_{\mathrm{FN}}$; otherwise same parameters as in Fig. 7.